For a chosen N and a suitably chosen high enough value of M, the results produced by Lawrence's method and the present method are indistinguishable.

V. Numerical Results

Table 1 lists the values of $dC_L/d\alpha$ and X_{ac}/C_r, where α is the wing incidence for various aspect ratios of rectangular and delta wings, as computed from Lawrence's method and the present method. The agreement is excellent. Although not tabulated here, similar excellent agreement exists for dg/dx in all cases.

However, when a check on the results plotted in Lawrence's paper was made, it was found that his dg/dx plots were in gross error for both rectangular and delta wings, which are clearly computational errors.

VI. Conclusions

A faster, accurate algorithm has been devised to solve the Lawrence equation for low-aspect-ratio wings. Errors of numerical computation occurring in Lawrence's original paper are noted.

References

[1]Lawrence, H. R., "The Lift Distribution on Low Aspect Ratio Wings at Subsonic Speeds," *Journal of the Aeronautical Sciences,* Vol. 18, Oct. 1951, pp. 683–695.

[2]Stark, V. J. E., "A Generalized Quadrature Formula for Cauchy Integrals," *AIAA Journal,* Vol. 9, Sept. 1971, pp. 1854–1855.

Experimental and Analytical Analysis of Grid Fin Configurations

Ross A. Brooks*
Rockwell International Missile Systems Division, Duluth, Georgia
and
John E. Burkhalter†
Auburn University, Auburn, Alabama

Introduction

AN unusual concept in missile fin design has led to a theoretical analysis and a series of subsonic wind-tunnel tests on grid fin configurations. The fin design, appropriately termed a "grid" fin, is an all-moveable fin that consists of (usually) high-aspect-ratio members of constant chord arranged in a grid-work pattern. The fin outer perimeter may be square, rectangular, octagonal, or virtually any shape consisting of straight members connected end to end, while the inner section of the fin may consist of any arbitrary grid pattern. The internal fin density may range anywhere from an open cavity to a dense honeycomb arrangement. Obviously, because of this flexibility, drag tailoring is easily obtainable. Additionally, these designs prove advantageous where control surfaces are span limited or situations where small actuator requirements are a high priority. Fins are normally mounted transverse to the longitudinal axis of the missile so that flow passes through the grid members. The angle of attack of the fin is achieved by a simple rotation of the fin about its horizontal axis in much the same way a conventional fin control surface is deflected.

The theoretical aerodynamic analysis of these grid fins logically lends itself to a vortex-lattice formulation. Primary coefficients of interest are normal force, root-chord bending moment, hinge moments, and drag. Vortex-lattice methods have been applied to complex configurations such as multiplanes, nonplanar wings, and entire aircraft lifting surfaces with intricate geometries, resulting in modern computerized methods such as those developed by Feifel[1] and Margason and Lamar.[2]

Theory

Standard vortex-lattice theory is centered around the Biot–Savart law and may be viewed as a constant-pressure paneling method suited to thin lifting surfaces of moderate to high aspect ratios. During the current investigation, a compressible vortex-lattice formulation was developed and embodied in a revision of the Biot–Savart law. In the analysis, the fin configuration is divided into a network of subpanels spaced uniformly (or nonuniformly) on each fin member in the spanwise and chordwise direction. A lifting vortex of unknown strength is located along the quarter-chord line of each subpanel as prescribed originally by Pistolesi[3] as the optimum location for spanwise vortices and later validated by Byrd[4] for chordwise vortices. A pair of trailing vortices is shed along the panel edges parallel to the uniform flow, downstream to infinity and forms a so-called horseshoe vortex.

The boundary condition of no flow through the surface is satisfied at the three-quarter-chord lateral center of each subpanel and, thus, completes Pistolesi's (1/4–3/4) theorem. Imposition of the boundary condition results in a system of equations that can be solved to yield the strengths of the vortices. Once the vortex strengths are known, the fin-sectional aerodynamic characteristics may be determined by appropriate summations of the chordwise direction. Finally, the total fin aerodynamic characteristics are computed by standard numerical integration techniques in the spanwise direction.

Vortex-lattice equations may be derived directly from the Biot–Savart equation, which defines the velocity induced at a field point by a vortex filament. In vector form, the linearized compressible form of this equation is

$$\bar{V}(x,y,z) = \frac{-\Gamma\beta^2}{4\pi} \int \frac{\bar{r} \times \overline{dl}}{|\bar{R}_\beta|^3} \tag{1}$$

where Γ is the filament strength, and $\bar{r}$ is the vector from a field point (x,y,z) to a differential length of the vortex filament $\overline{dl}$. Compressibility enters the equation through a typical Mach number term in the numerator ($\beta^2 = 1.0 - M_\infty^2$) and through the elliptic radius defined by

$$|\bar{R}_\beta| = \{(x-x_o)^2 + \beta^2[(y-y_o)^2 + (z-z_o)^2]\}^{0.5} \tag{2}$$

The boundary conditions of no flow through the fin at control points can be written in matrix notation as

$$[A]\,(\Gamma) = [B] \tag{3}$$

The $[A]$ matrix is known as the influence matrix and is composed of the downwash terms given by Eq. (1). The $[B]$ matrix is governed by the angle of attack and any other known upwash or downwash terms, and for the present case is simply

$$B_i = (\sin\alpha)_i, \qquad i = 1, nc \tag{4}$$

where nc is the total number of grid-fin control points. Once the vortex strengths are found by matrix algebra, the aerodynamic characteristics of the lifting surface may be computed through utilization of the Kutta–Joukowsky theorem for the

Received Feb. 17, 1988; revision received Jan. 15, 1989.

*Member, Technical Staff. Member AIAA.

†Associate Professor, Department of Aerospace Engineering. Member AIAA.

sectional properties, followed by numerical integration in the spanwise direction for total coefficients.

The sectional properties for a grid fin are obtained by making imaginary vertical slices at predetermined spanwise stations. The strengths of all vortices cut by a single imaginary plane are summed to give the sectional property value at the particular spanwise station. For the case when a particular vortex is inclined with respect to the positive y axis, an appropriate component of the vorticity strength is summed. Summing a "component" of the vorticity strength is justified when the panel is inclined to a given axis. The spanwise stations must be selected so that no station fails on a trailing leg. The hinge-moment coefficient is computed about the fin axis, which passes through the chord midpoint.

Results and Conclusions

Verification of the theory as described was demonstrated by comparison with experimental wind-tunnel data. Data were obtained for eight different grid-fin geometries. Four models consisted of a 7.62×7.62-cm square outer shell and the remaining four models had a 7.62×15.24-cm rectangular outer shell. All fin models had a 2.54-cm constant chord length and all fin grid elements were approximately 0.064-cm thick. The fin models were tested at a dynamic pressure of approximately 7.62 cm of water, which corresponded to a speed of about 36.6 m/s. Force and moment coefficients were based on a reference length of 7.62 cm and a reference area of 45.62 cm^2. The average Reynolds number based on the chord length of 2.54 cm was 165,000. Obviously, at this tunnel speed, the flow is incompressible and, therefore, compressibility terms in the induced-velocity equations are not necessary as they would be at higher flow rates.

Wind-tunnel test data for the grid fins demonstrated several interesting trends. As would be expected, horizontal slat configurations tend to provide higher normal-force characteristics than open geometries, although structural limitations may reduce the practical effectiveness of such designs. These configurations would be suited to span-limited situations where

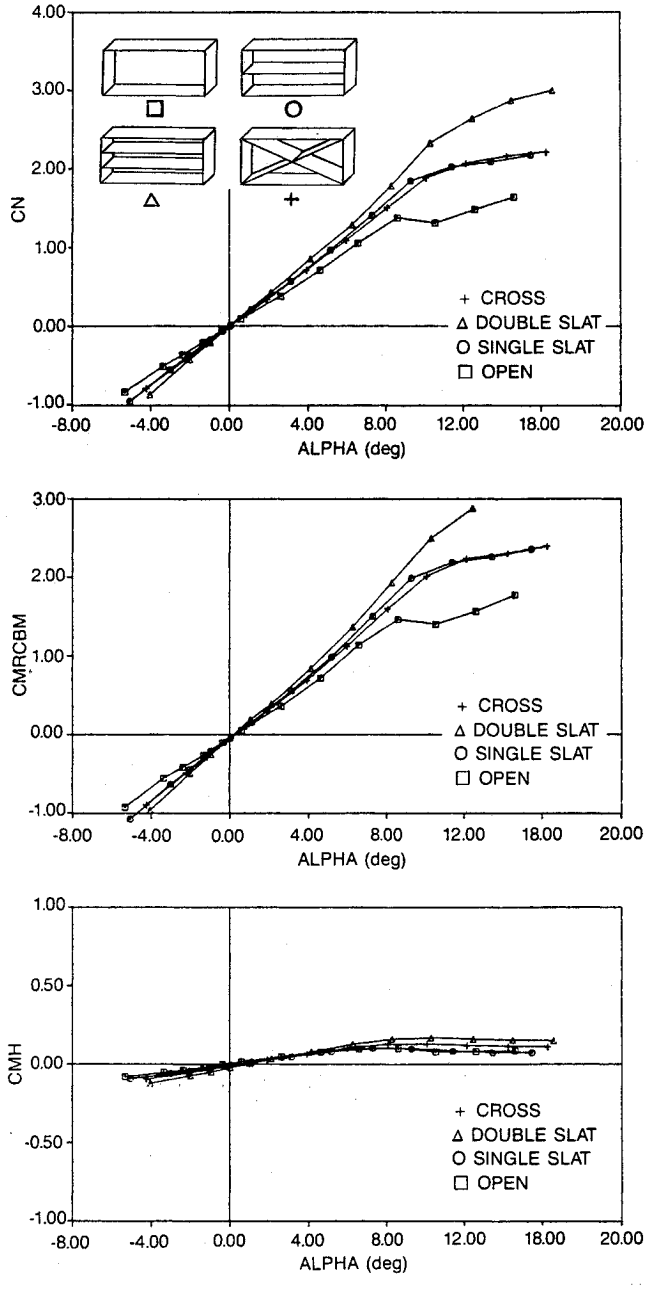

Fig. 1 Grid-fin aerodynamic coefficients vs angle of attack for the four 7.62×15.24-cm fins (CN = normal force; CMRCBM = chordwise bending moment at root; and CMH = hinge moment).

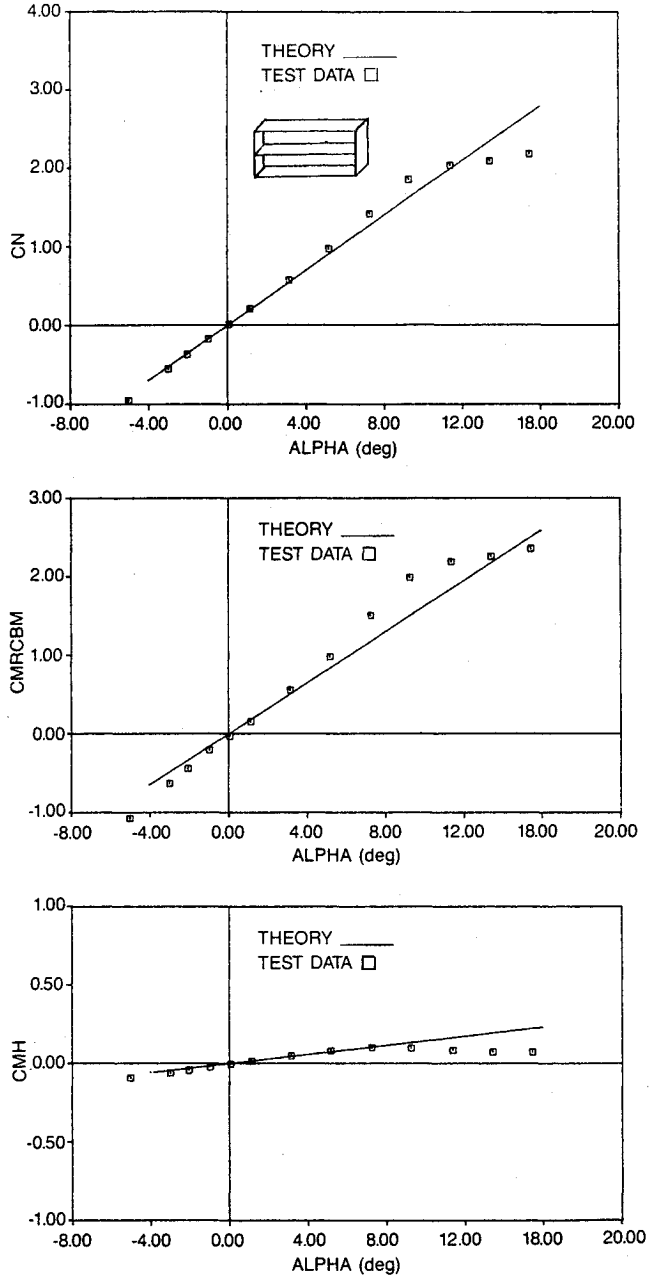

Fig. 2 Normal-force, root-chord bending moment, and hinge-moment coefficients vs angle of attack for the 7.62×15.24-cm single-slat fin.

more slats (lifting surfaces) could be added to a particular fin to attain a desired normal force. Complex grid-like inner fin arrangements provided increases in normal force over open geometries and a comparatively larger axial force, and may be suited to applications requiring high structural integrity, well-behaved lift characteristics, and high drag.

Results presented in Figs. 1 and 2 indicate typical characteristics of grid-fin configurations. For both cases, the square and the rectangular configurations, there is a significant increase in normal force at higher angles of attack as additional slats are added. As expected, the double-slat fin produced larger normal forces. However, the single slat and cross fins, at least over the linear range, generated approximately the same normal forces even though the cross fin had a larger lifting surface area. The 7.62×15.24-cm grid fins exhibited similar trends. Thus, the cross-configuration fin of both sizes produce roughly the same normal force as the single slat fin, and could be tailored to produce a "desired" axial force as well as a desired normal force by designing for a certain number of effective horizontal slats. These same fins, because of their low hinge actuator requirements, may be efficient as lifting surfaces when flown in the normal transverse direction but may also be used as "drag" brakes if turned to a horizontal position.

The internal arrangement of a particular grid fin appears to also influence the stall point. Generally, the more complex an internal arrangement is, the higher the stall angle of attack. As a matter of fact, for the more complex geometries, the cross and double, the stall does not occur below 18-deg angle of attack. Hinge moments (CMH) for all cases are very small and root-chord bending moments (CMRCBM) exhibit properties similar to the normal-force behavior.

Agreement between theory and experimental data was quite good for all configurations with typical results shown in Fig. 2. It is interesting to note that the slope of the C_N-alpha curve tends to increase up to approximately 8.0 deg to such an extent that the theory underpredicts the data slightly in this region, which is atypical for vortex-lattice formulations. In this case, it appears that the upper "slat" stalls before the lower slat, which produces a distinct "bump" in the aerodynamic coefficients between 4.0 and 10.0-deg angle of attack. Past 10–12 deg, there seems to be a second "stall," perhaps of the bottom or cross members. Results were very repeatable and both multiple slats and cross-slat configurations exhibited the same trends.

Tests were not run at angles of attack higher than 18 deg, so that in some cases the actual stall of the fin was never observed. Tuff tests did, however, show that the upper fin members do indeed stall with separated (reverse) flow on the top side of the upper slat. These same tests also showed that bottom slats did not stall at least up to 18-deg angle of attack. For all configurations, the hinge moments were very small and increased only slightly with angle of attack. In some cases, the slight increase was followed by a decrease in CMH, probably as a result of secondary fin-element stall. Although one cannot be certain, it appears that most of the hinge-moment contribution comes from the fact that at higher angles of attack, the lower slats (unstalled) normal-force contribution is in front of the hinge line, while the upper (stalled) normal-force contribution is behind the hinge line. Very little of the hinge moment comes from the fact that on each fin element the center of pressure is in front ($\approx$quarter-chord) of the hinge line.

References

[1]Fiefel, W. M., "FORTRAN IV—Program zur Berechnung von V—Leitwerken," Mitteilang im Institut für Aerodynamik and Gasdynamik der Technishen Universität, Stuttgaart, FRG, 1966.

[2]Margason, R. J. and Lamar, J. E., "Vortex-Lattice FORTRAN Program for Estimating Subsonic Aerodynamic Characteristics of Complex Planforms," NASA TN D-6142, 1971.

[3]Pistolesi, E., "Considerations of the Mutual Interference of Airfoil Systems," L. G. L. Rept., 1937, pp. 214–219.

[4]Byrd, P. F., "Erganzung zu dem Autsatz von N. Scholz, Bietrage zur Theoria der Tragenden Flache," *Ing.-Arch. Bd.* XIX, Heft 6, 1951, pp. 321–323.

Transition Limits for Water-Droplet Crystallization with the NASA Lewis Icing Nozzle

C. John Marek*
NASA Lewis Research Center, Cleveland, Ohio

Introduction

SINCE ice accumulation on aircraft and engine surfaces can seriously degrade performance, icing tests are an important aspect of the development and verification tests of aerospace flight systems. The ultimate goal of a ground-based test facility is to effectively simulate icing conditions actually encountered by an aircraft in flight.

To produce the small droplets for icing-cloud simulation, high-pressure air-atomizing nozzles are used. For certain icing-test applications, such as model scaling, median drop sizes down to 5 μm are needed, which may require air-atomizing pressures greater than 3000 kPa. Isentropic expansion of the atomizing air from this pressure to atmospheric pressure results in airstream temperatures of -160°C, which will result in ice crystals forming in the cloud unless the air and water are heated to high initial temperatures.

The purpose of these tests was to determine the effect of atomizing air temperature and pressure on the formation of ice crystals.

The NASA Lewis standard icing spray nozzle, shown in Fig. 1, was selected because it has been extensively calibrated and is currently used in the NASA Lewis Icing Research Tunnel. The tests were conducted in the single nozzle icing research test cell at Arnold Engineering Development Center with the nozzle spraying into a bellmouth followed by a 0.91-m-diam duct. The distance from the nozzle to the measuring station was 4.42 m.

During the test, the drop-size distribution was determined with the Laser Fiber Optic System (FOS). The FOS uses a single laser beam and measures the shadow of the particle with a lens system and row of photomultiplier tubes.

A "soot slide" technique as described by Skidmore and Pavia[1] was used to indicate the presence of crystals. The impressions of the droplets in the soot coating are indicative of the state, liquid or crystal, of water droplets. A more complete description of the technique is given in Ref. 2.

Results

The effect of atomizing air temperature on droplet crystallization was evaluated by setting the atomizing air pressure between 300 and 830 KPa and lowering the atomizing air temperature from 115 to 15°C. Tests were conducted at tunnel temperatures of -13 and -8°C. Most of the tests were conducted at a spray-nozzle water temperature of 60°C. The tunnel Mach number was 0.3 and the liquid water content (LWC) was 0.6 g/m^3 for all of the tests.

The tunnel and spray conditions were set and a soot slide was exposed and examined under the microscope for the pres-

Presented as Paper 88-0289 at the AIAA 26th Aerospace Sciences Meeting, Reno, NV, Jan. 11–14, 1988; received April 22, 1988; revision received Feb. 28, 1989.

*Senior Aerospace Engineer, Aerothermochemistry Branch, Internal Fluid Mechanics Division.